Biomedical Signal Processing and Control 101 (2025) 107083

Contents lists available at ScienceDirect

Biomedical Signal Processing and Control

journal homepage: www.elsevier.com/locate/bspc

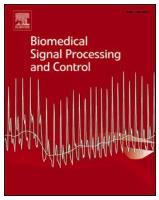

Semi-Supervised anomaly detection for the prediction and detection of pediatric focal epileptic seizures on fused EEG and ECG data

Apostolos Karasmanoglou [a,*], Giorgos Giannakakis [b,c], Pelagia Vorgia [d], Marios Antonakakis [e,a], Michalis Zervakis [a]

[a] School of Electrical and Computer Engineering, Technical University of Crete, Chania, Greece
[b] Institute of Computer Science Foundation for Research and Technology – Hellas, Heraklion, Greece
[c] Department of Electronic Engineering, Hellenic Mediterranean University, Chania, Greece
[d] Agri-food and Life Sciences Institute Hellenic Mediterranean University, Heraklion, Greece
[e] Institute for Biomagnetism and Biosignal Analysis, Muenster, Germany

ARTICLE INFO

Keywords:
Multi-modal Anomaly Detection
Seizure Detection
EEG
ECG
HRV
Epilepsy

ABSTRACT

We introduce a semi-supervised multi-modal anomaly detection framework for efficient seizure prediction and detection in pediatric patients suffering from focal epilepsy. Our approach combines temporal, spectral and nonlinear features derived from two modalities: Electroencephalogram (EEG) recordings recorded in electrodes placed adjacent to the seizure loci and Electrocardiogram (ECG) recordings from which we derive Heart Rate Variability (HRV) parameters. We employ anomaly detection models, such as the Minimum Covariance Determinant (MCD) estimator, Isolation Forest (IsF), One-Class Support Vector Machine (OCSVM), and Local Outlier Factor (LOF), which were trained in a semi-supervised way to identify EEG / HRV anomalies during or prior to seizure onset. Our method demonstrates robust performance in detecting segments of ictal activity, achieving ROC-AUC scores of up to 95% using patient-specific thresholds and 91% using patient-in specific thresholds. Additionally, our framework was able, in most cases, to anticipate seizures 16–23 s prior to seizure onset, with a minimal duration of false warnings. These findings support the potential for developing a lightweight, wearable EEG / ECG monitoring device optimized for pediatric patients.

1. Introduction

Epilepsy is a neurological disorder characterized by sudden disruptions in normal brain activity, which manifest in seizures, affecting approximately 50 million people worldwide [1 2]. Focal epilepsy, also known as partial epilepsy, is a type of epilepsy characterized by bursts of electrical activity that originate in a specific, localized neuronal net of the brain [3]. The nature and symptoms of focal epilepsy can vary widely depending on the specific neuronal net of the brain affected by abnormal electrical activity [4], making it particularly difficult to diagnose and treat. Frontal lobe focal epilepsy, in particular, poses unique diagnostic challenges due to its varied seizure symptoms, often misinterpreted as behavioral or psychiatric disorders [5], and its frequent occurrence during sleep, which can be mistaken for sleep disorders [6].

These difficulties are exacerbated in cases involving pediatric patients. Focal seizures in children often present unique challenges in diagnosis and management. Its manifestations can be subtle and easy to overlook or misinterpret, such as atypical behaviors or cognitive changes [7]. Unlike adults, treatment methods for pediatric patients with focal epilepsy are not well established and require careful monitoring. Treatment options may involve medication, diet changes and possibly surgery, all adapted to actively developing brains [8].

Presurgical diagnosis of focal epilepsy poses a significant challenge, necessitating accurate detection of seizures. The most well-established and adopted modality towards this direction is the Electroencephalogram (EEG), the analysis of which constitutes an intricate task demanding both rigorous effort and specialized expertise [9,10]. In response to this challenge, various machine learning approaches have been developed for the automatic detection of seizure-related abnormalities in EEG [11]. Additionally Recent strides in medical and machine learning research have unveiled the potential of ECG derived features like Heart Rate Variability (HRV) metrics as a valuable tool for

* Corresponding author.
E-mail addresses: akarasmanoglou@tuc.gr (A. Karasmanoglou), ggian@ics.forth.gr (G. Giannakakis), vorgia.pedia@gmail.com (P. Vorgia), mantonakakis@tuc.gr (M. Antonakakis), mzervakis@tuc.gr (M. Zervakis).

https://doi.org/10.1016/j.bspc.2024.107083
Received 26 June 2024; Received in revised form 1 October 2024; Accepted 14 October 2024
Available online 26 November 2024

early detection of seizure-related anomalies [12].

A recent trend in automatic seizure detection research is the fusion of EEG and ECG modalities for enhancing performance. Qaraqe et al. [13] investigated different methods for fusing temporal and spectral EEG and ECG features, using a Support Vector Machine (SVM) classifier. Their study was conducted on seizure data from 10 patients, successfully detecting all seizures with the amount of errors ranging from 1 to 7 false alarms per hour. Mesbah et al. [14] conducted a study on classifying 13 neonatal patient seizures fusing multi-channel EEG and ECG features from the time, frequency and time–frequency domains using a linear classifier, outperforming similar unimodal classifiers and achieving remarkable performance scores: 95.20 % sensitivity & 88.60 % specificity. Vandecasteele et al. [15] investigated behind-the-ear EEG and ECG fusion developing a patient-specific SVM classifier which achieved increased sensitivity of up to 92 %at the same false alarm rate compared to a unimodal classifier in a database consisting of 42 patients. In a more recent study, Sigsgaard et al [16] presented a random forest-based multi-modal binary classifier for seizures, utilizing OR-rule fusion of the EEG and ECG modalities, that was able to detect all seizures in 10 out of 14 patients of the Siena dataset with an average delay of 19 s. As an overall estimation of the current state of the art Westrhenen et al. [17] conducted a review of 21 studies which revealed that multimodal approaches significantly outperform unimodal algorithms in reducing false alarm rates.

Practical deployment of these methodologies, however, still faces considerable challenges. Patient-specific deployment requires prior recordings of seizures for model fitting, leading to enrollment difficulties and strenuous recording sessions in which a sufficient number of seizures needs to be recorded. This data collection may be particularly strenuous in the case of pediatric patients. Patient-agnostic deployment on the other hand relies on large datasets, demanding extensive and ethically cleared data acquisition sessions. Patient agnostic deployment may be ineffective overall, as many studies report contradictory or inconclusive findings regarding their physical effects with results seemingly varying depending on seizure type and localization / lateralization [18,19,20,21,22,23]. Additional challenges include: the subjective or erroneous labeling of ictal events [24,25], the inherent non-stationary and non-linear properties of EEG and Heart rate dynamics [26,27], as well as their patient-specificity [28,29].

In light of these advancements and the challenges they face, we propose a semi-supervised, multi-modal anomaly detection framework aimed at enhancing both seizure prediction and detection. The term semi-supervised refers to the nature of the models, which requires only data samples from the inlier class [30,31]. In both unsupervised and semi-supervised anomaly detection, training may be conducted on unlabeled data. We distinguish semi-supervised from unsupervised anomaly detection, in that the former is trained on an inlier-exclusive set, which constitutes in our view a form of supervision. In this context our models are trained on only seizure-free EEG and ECG data and can then detect deviations from this typical brain and cardiac activity. Fig. 1 shows a diagram that helps distinguish between different training schemes, including the proposed semi-supervised scheme. This aspect addresses the data collection concerns we mentioned previously, as model deployment is possible with no prior knowledge of EEG/HRV ictal activity patterns and are easily trained on a small set of normal EEG/ECG data. Furthermore, it allows us to train models tailored to each patient's specific EEG and Heart Rate dynamic. The models we propose are inherently sensitive to novelty, allowing for the detection of a wide set of potential abnormalities corresponding to different types of epileptic conditions. In our pipeline we utilize a rich set of EEG and HRV features, including non-linear features which can capture non-linear and non-stationary properties of the signal. We investigate fusing these features using various fusion techniques to enhance seizure prediction and detection. Our approach utilizes a small set of sensor channels, allowing for potential integration into portable and wearable devices for remote monitoring [32,33].

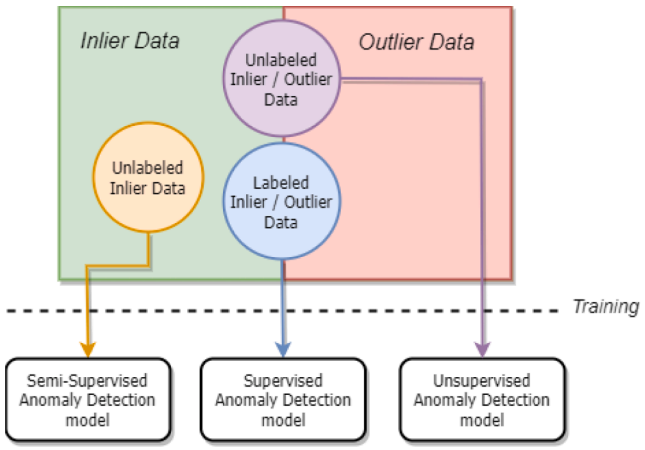

Fig. 1. Distinction between supervised, semi-supervised and unsupervised anomaly detection in the context of seizure-related anomaly detection.

Our models are trained and tested on pediatric patients with focal epilepsies, localized around the frontal lobe. Our system is primarily targeted for application on the pediatric population as it addresses key challenges specific to it. Limited data availability is a major concern, as collecting extensive EEG / ECG recordings in children is difficult due to ethical constraints and their high activity levels [34]. Our semi-supervised approach, requiring only normal data for training, effectively combats this limitation. Additionally, pediatric patients exhibit significant patient-specific variability in EEG and heart rate dynamics due to ongoing neurological development [35,36], which our patient specific framework is ideal for. Moreover, the need for minimally invasive, lightweight and portable monitoring is critical in this demographic [37]. Our system's compatibility with portable and wearable devices provides the potential for comfortable, long-term observation without disrupting the daily activities of young patients. Specifically, the dataset we utilize is limited to patients with frontal lobe epilepsy, which allows us to investigate a specific type of lightweight electrode configuration centered around the locus in which the seizures originate, consistently across patients.

2. Materials and methods

2.1. Dataset

This study's dataset included 7 pediatric participants (3 females) with an average age of 8.0 ± 4.4 years at the time of monitoring, diagnosed with frontal lobe focal epilepsy. The recorded dataset included 29 seizures in total.

All participants experienced movements during seizure. All patients except 2 were taking medication at the time of the recording session. The dataset contained annotations indicating the start/end of the seizures performed by an expert pediatric neurologist. All participants provided informed consent. The study was approved by the Ethics Committee of Research of the Technical University of Crete (approval no. 56/08–12-2022). A summary of the utilized dataset's subjects is included in Table 1.

2.2. Data Preperation

2.2.1. Pre-processing

EEG signals were digitized at a sampling frequency of 256 Hz, Independent Component Analysis (ICA) was used to suppress artifacts and noise related to the subject's activity [38].

The ECG signal was sampled at a frequency of 256 Hz synchronously to the EEG. Furthermore, it was detrended and subjected to bandpass filtering to eliminate power line interference. A dynamic threshold

Table 1
Study population demographics and seizure types.

Patient Code	Total seizures	Recording minutes	Age	Sex*	Epilepsy	Under medication	Movement during seizure
PAT_13	1	92	9	Female	focal right frontal lobe	yes	yes
PAT_14	8	378	7	Female	focal right frontal lobe.	yes	yes
PAT_15	1	90	13	Male	focal fronto-polar lobe	yes	yes
PAT_24	13	362	10	Female	focal left frontal lobe	yes	yes
PAT_27	4	442	13	Male	focal right frontal lobe	no	yes
PAT_29	1	96	0	Male	focal bifrontal lobe	yes	yes
PAT_35	1	98	4	Male	focal	no	yes
Total seizures	**29**						

* The term "sex" here refers to sex assigned at birth.

based on neighborhood envelope was implemented to diminish artifacts [39].

After obtaining the preprocessed ECG signal, the R peaks –were identified and the sequence of the RR −Intervals (RRI) were extracted. Ectopic heartbeats are removed from the RR series as artifacts, for this purpose, we employed the method detailed in [40], where a heartbeat is classified as ectopic if it shows a percentage change of 40 % compared to the average of the previous five heartbeats.

2.2.2. Data selection

An important consideration is identifying which segments of the recordings should be included in the analysis. Research indicates that the duration of the post-ictal phase can vary significantly depending on the type of seizure, ranging from 10 to 30 min to as long as 5–6 h in some instances [41,42]. In this study, post-ictal periods, which maintain HRV statistical characteristics akin to the ictal phase, were excluded from the analysis. Also, several seizure cases were omitted due to the brevity of their interval to the previous seizure of the subject. Moreover, sleep periods within interictal phases were also removed due to the influence of sleep stage transitions and micro-arousals on HRV parameters. Other segments excluded encompassed moments like removing the EEG apparatus for bathroom breaks, lunch breaks, instances of significant physical movement, and when participants (specifically children) interfered with or removed the electrodes, identified via video recordings. The baseline period was meticulously chosen as an interictal phase, devoid of seizure activity, to ensure the analysis was conducted on appropriate data segments. Consequently, the data ultimately analyzed in this study adhered to these criteria to exclude unsuitable segments, clearly delineating the pre-ictal, ictal, and postictal periods. This selection procedure resulted in a dataset including a total of 29 focal seizures.

2.2.3. Preparation for feature extraction

In each one of the 29 cases we first isolated a 10-minute time-segment of ECG and EEG before the seizure onset. Subsequently, the data from seizure and pre-seizure intervals were separated and split into training and test sets. The training set was comprised of strictly pre-ictal data segments, whereas the test set contains both ictal and pre-ictal segments for evaluation. If multiple seizures occur within a 10-minute period, only the data from the seizure at the 10-minute mark is included, while the data from the other seizures within that timeframe is omitted. This means that length of the pre-ictal interval as well as the size of the training data may vary across cases.

We utilized 19-channel scalp EEG recordings according to the international 10–20 system. However, we investigated the possibility of a smaller subset of channels, with 7 electrodes (Fp1, Fp2, F7, F3, Fz, F4, F8) adjacent to the seizure locus to serve a more lightweight configuration and to further increase the signal-to-noise ratio (SNR). The time series data from each modality are interpolated for a range of timepoints, using a fixed step of one second. The timepoints at which we interpolate both modalities are the same, ensuring alignment when fusing them.

2.2.4. EEG feature extraction

The EEG signal was divided into overlapping segments of 2 s segments with a step of 1 s between successive segments for feature extraction. We utilize multiple kinds of EEG features for efficient epileptic seizure detection.

Hjorth parameters, including activity, mobility, and complexity [40], are effective biomarkers in detecting seizures from EEG signals [43]. In order to capture Gamma Band activity [44,45,46] we include the percentage of the power in the signal's PSD from a high frequency band (30–120 Hz) as a feature. To deal with the inherent non-linearity and non-stationarity of EEG dynamics nonlinear features such as Decorrelation [47], Fractal Line Length (FLL) [48,49] and Lempel-Ziv Complexity (LZC) are utilized, tailored for the purposes of seizure EEG analysis and onset prediction [47,48,50,48].

2.2.5. HRV feature extraction

HRV features were extracted from the RR series using time segments corresponding to 1 min of the interpolated RR series shifted by one second. The HRV features were categorized into time, frequency and non-linear measures, each one demonstrating specific characteristics of cardiac activity [51]. In our pipeline we have selected a diverse set of HRV features.

Common time-domain and frequency domain features are extracted from the RR series, reflecting various physiological processes [52]. In addition to these, a set of non-linear features are utilized to capture non-linear and non-stationary properties of the RR series. The Poincare Plot, a common nonlinear feature, assesses sympathetic-parasympathetic nervous system activity [53]. Recurrence Quantification Analysis (RQA) features examine recurrence patterns in RR data, capturing heart rate dynamics [54] with a demonstrated potential in predicting seizure onset [55]. Multifractal Detrended Fluctuation Analysis (MFDFA) [56 57], assesses multifractality in RR series patterns which may be useful in detecting pathological conditions [58,59]. Additionally, series entropy approximations like Sample entropy [60] and Attention entropy [61] assess irregularity and complexity of RR series patterns.

The EEG and ECG features extracted in this study are summarized in

Table 2
EEG / HRV Features utilized in anomaly pipeline.

EEG		
Hjorth parameters		Activity, Mobility, Complexity
Spectral		30–120 Hz Frequency band power
Non-linear		Fractal Line Length, Decorrelation, Lempel-Ziv Complexity
HRV		
Time domain		RMSSD, NN50, Average ΔNNI, SDSD, Triangular Index
Frequency domain		Total Power, Relative VLF, Relative LF, Relative HF, VLF peak, LF peak, HF peak, LF/HF
Non-linear	**Poincare**	SD1, SD2, Ellipse Area, SD1-SD2 Ratio
	RQA	Recurrence Rate, Diagonal Recurrence, Divergence, Determinism, Laminarity, Determinism-Recurrence Ratio, Trapping Time, Average Diagonal, Diagonal Entropy
	MFDFA	Mean, Max, Width, Peak, Asymmetry (AR), Delta, Fluctuation (hFI), Increment (hCf)
	Entropy	Sample Entropy, Attention Entropy

Table 2. In total our models leverage feature vectors of 36 dimensions for the ECG modality and 49 dimensions (= 7 channels × 7 features) for the EEG when using the frontal channel configuration, we describe.

2.2.6. Anomaly detection models

Anomaly detection involves identifying events that significantly deviate from the expected or normal behavior within a dataset. It can be defined mathematically as the task of identifying outlier data points that belong to a feature space $X \subset \mathbb{R}^N$. The set X can be expressed as a union of disjoint sets $X = X_{inliers} \cup X_{outliers}$, where $X_{inliers}$ is characterized by a typical pattern whereas $X_{outliers}$ represents the subset of data that exhibits uncommon or unexpected characteristics. In general, $X_{inliers}$ tends to be a bounded set of clustered datapoints in the feature space, whereas $X_{outliers}$ can span an infinite range. The goal of an anomaly detection model is to distinguish anomalies from the majority of data points that conform to a typical pattern. The model essentially serves as a score function $s : \mathbb{R}^N \rightarrow [0, +\infty)$ that quantifies how anomalous a datapoint is. For each model we utilized, we provide a short summary of its mathematical formulations.

The models we utilize in our pipeline are the Minimum Covariance Determinant (MCD) [62], Isolation Forest (IsF) [63].

One-Class SVM (OCSVM) [64], and the Local Outlier Factor (LOF) [65]. Details on these models are included in Appendix A.

2.2.7. Anomaly detection on fused EEG and ECG modalities

Multi-modal anomaly detection involves the synergy of data collected from multiple sources or modes to detect anomalous patterns, developing a robust system that leverages a richer set of information from these modes. In this work, synchronized ECG and EEG recordings comprise these modes. This is achieved through the fusion of features extracted from each modality, which we will symbolize as $\mathbf{x}_{HRV} \in \mathbb{R}^{N_{HRV}}$, $\mathbf{x}_{EEG} \in \mathbb{R}^{N_{EEG}}$. The processes involved in such a multi-modal anomaly detection pipeline are presented in Fig. 2.

Two primary fusion strategies are commonly employed: early (data-level) feature fusion and late (decision-level) feature fusion [66]. Early feature fusion, denoted as Φ_{early}, integrates information from both modalities by concatenating and standardizing feature vectors derived from each modality prior to model fitting. This joint feature vector can then be used for fitting an anomaly detection model. Such a model can be represented as:

$$\Phi_{early}(\boldsymbol{x}_{HRV}, \boldsymbol{x}_{EEG}) = s(c(\boldsymbol{x}_{HRV}, \boldsymbol{x}_{EEG})), \tag{1}$$

Where $c : \mathbb{R}^{N_{HRV} \times N_{EEG}} \rightarrow \mathbb{R}^{N_{HRV}+N_{EEG}}$ denotes the concatenation-standardization operation and $s(.)$ is the scoring function of some model trained on the multi-modal data. Late feature fusion, denoted as Φ_{late}, combines unimodal anomaly scores from each modality. In the late fusion strategy, the anomaly scores obtained from each modality are combined using various aggregation functions, such as minimum, maximum, and summation:

$$\Phi^{min}_{late}(\boldsymbol{x}_{HRV}, \boldsymbol{x}_{EEG}) = min\{\Phi_{HRV}(\boldsymbol{x}_{HRV}), \Phi_{EEG}(\boldsymbol{x}_{EEG})\}, \tag{2}$$

$$\Phi^{max}_{late}(\boldsymbol{x}_{HRV}, \boldsymbol{x}_{EEG}) = max\{\Phi_{HRV}(\boldsymbol{x}_{HRV}), \Phi_{EEG}(\boldsymbol{x}_{EEG})\}, \tag{3}$$

$$\Phi^{SUM}_{late}(\boldsymbol{x}_{HRV}, \boldsymbol{x}_{EEG}) = \Phi_{HRV}(\boldsymbol{x}_{HRV}) + \Phi_{EEG}(\boldsymbol{x}_{EEG}). \tag{4}$$

2.2.8. Warning generation

In this section, we outline our proposed methodology for generating real time warnings using the trained models. Warning generation relies on the precise setting of thresholds regarding sustained scores over a series of successive feature segments. A visual representation of the interplay between a score threshold and the duration for which the data generates scores surpassing it is displayed in Fig. 3. Our analysis yields a decision methodology for generating warnings that minimizes latency and false positives.

We first define a score threshold s_c, which indicates considerable anomaly detected in the data. Our datapoints are time-ordered feature vectors which we will denote by $\boldsymbol{x}_t$, temporarily disregarding their modality of origin. Consider a set of continuous segments of time during which the anomaly score of data points is over the threshold:

$$A_k(s_c) = \{t \in [t_k, t_{k+1}] \,|s(\boldsymbol{x}_t) \geq s_c\}, k = 1, \cdots, K. \tag{5}$$

$$d(A_k) = t_{k+1} - t_k. \tag{6}$$

We define a time threshold t_c which signifies the minimum amount of time that the anomaly score needs to stay above the threshold to generate a warning. Accordingly, warnings are generated at time points:

$$T_w = \{t_k + t_c | d(A_k) > t_c\}. \tag{7}$$

There is a notion in which a warning can be false or true, in that it

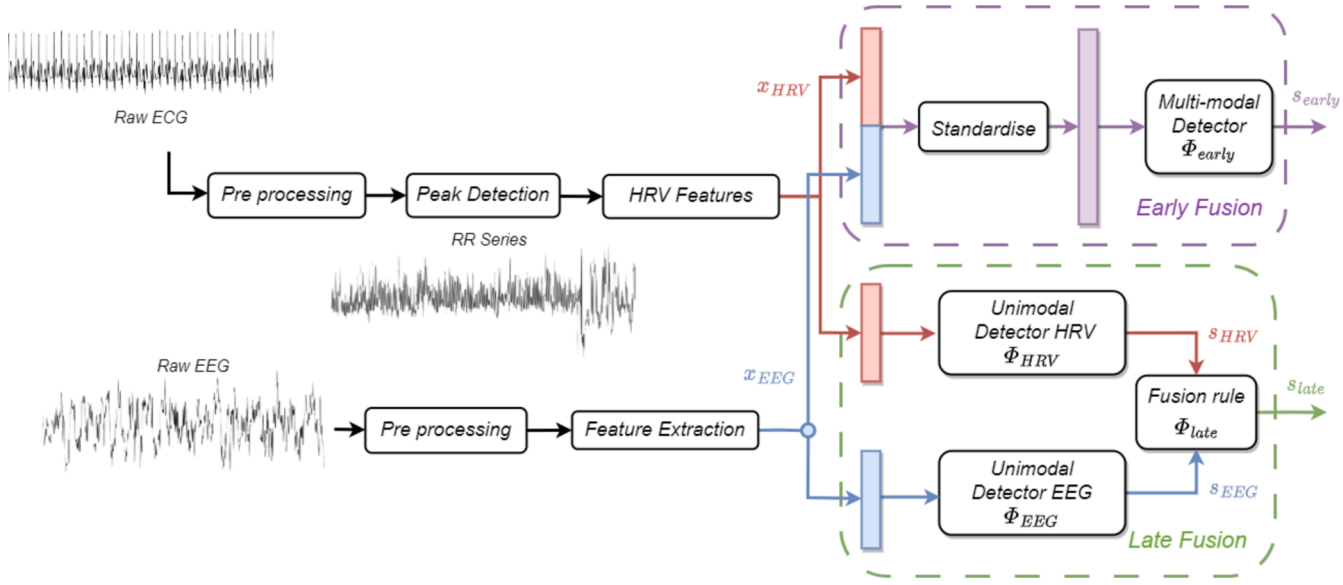

Fig. 2. A sketch of the Fused ECG/EEG anomaly detection pipeline. Features are extracted from segments of both modalities (EEG and ECG). Models are trained separately on each modality when implementing early fusion or on both when implementing early fusion ($\Phi_{HRV}, \Phi_{EEG}, \Phi_{early}, \Phi_{late}$). The models then provide scores ($s_{HRV}, s_{EEG}, s_{early}, s_{late}$) for each segment which are indicative of novel and potentially abnormal activity.

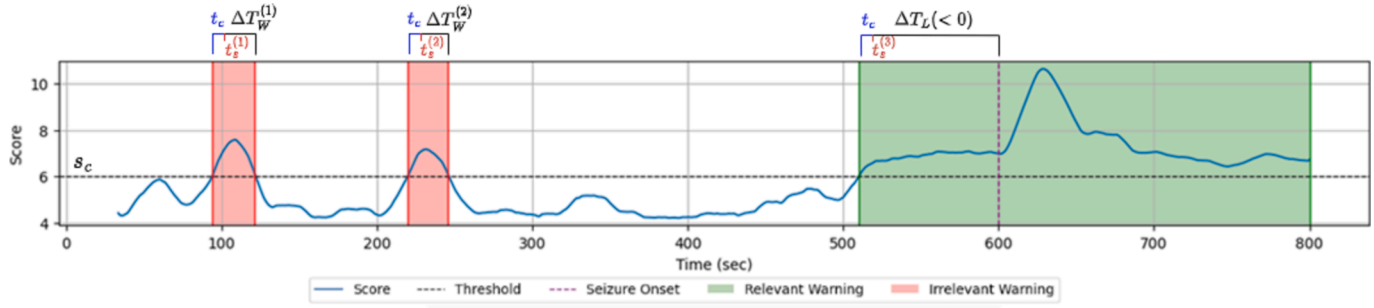

Fig. 3. Example showcasing the warning generation procedure, using arbitrarily set score and time thresholds. The anomaly score assigned to each segment is compared to the score threshold s_c. If it exceeds this threshold for a duration longer than the time threshold t_c then a warning is generated. In the illustrated example two false warnings of duration $\Delta T_W^{(1)}$ and $\Delta T_W^{(2)}$ are issued at times $t_s^{(1)}$, $t_s^{(2)}$. Finaly, at time $t_s^{(3)}$ a correct warning is generated, prior to the seizure onset by ΔT_L seconds. The two thresholds can be adjusted appropriately to minimize false warning duration and latency.

corresponds to a physically observable abnormality that is manifesting or occurring at the time of warning, which in our instance is the seizure. Consider the index set $I = \{1, 2, \cdots, K\}$. We define two subsets of the index set based on whether they index a false or true warning-producing segment containing a segment of ictal activity:

$$I_F = \{k \in I | A_k \cap E = \emptyset, d(A_k) > t_c\}, \tag{8}$$

$$I_T = \{k \in I | A_k \cap E \neq \emptyset, d(A_k) > t_c\}, \tag{9}$$

where $E = [t_{start}, t_{stop}]$ is the time segment in which the seizure event occurs. According to this formulation, we can quantify the latency or lead time of the warning as:

$$\Delta T_L(s_c, t_c) = \min_{k \in I_T}\{t'_k \in T_W\} + t_c - t_{start}, \tag{10}$$

indicating how many seconds after (latency) or before (lead time), in case of negative sign, the seizure a related warning arrives. We may also define the total duration of false warnings as:

$$\Delta T_{FW}(s_c, t_c) = \sum_{i \in I_F} d(A_i) - t_c, \tag{11}$$

We encounter the problem of setting s_c, t_c for each model and patient case in order to jointly minimize them. This can be seen as a *meta*-problem of score-based anomaly detection.

To address this, we conducted a post-hoc investigation on setting the optimal s_c, t_c thresholds using our available data. Since our aim is to minimize two objectives, and we deem the false positive duration to be the hinge of our systems trustworthiness, we select this quantity as the constraint, setting the levels of acceptable false positive duration α as percentages of the total recording duration prior to the seizure, and minimizing the latency within this constraint level:

$$\min_{s_c, t_c} \Delta T_L(s_c, t_c) \tag{12}$$

$$\text{s.t}\ \Delta T_{FW}(s_c, t_c) \leq \alpha \cdot (t_{sz} - t_0).$$

The process involves selecting a subsample of the pre-ictal data points contained in a single case recording and using them to train a model. The model is then evaluated on the entire case data. Anomaly scores are derived and fed into an accumulator function (moving average). Based on these scores, the optimal s_c, t_c pair is extracted considering the warning latency and false positive duration that would be produced if the system were deployed in real time. The procedure is repeated 50 times for each percentage level. From these trials, we derive the average latency, false positive duration, and optimal thresholds for score and time.

2.2.9. Evaluation

To evaluate the detectors, we divide the dataset into two subsets: one containing features of normal EEG/ECG data and the other with seizure data. The evaluation process employs a 10-fold cross-validation scheme on the normal data. The detector is trained on nine folds of inliers, and the remaining fold is used for testing, along with the seizure data. Since we assume no outliers in the training set, the thresholds for detection cannot be determined during model training and must instead be set post-hoc. We present two different analyses: case-specific optimal thresholds and a global (case-in specific) optimal threshold analysis. For the case-specific analysis, we set a threshold specific to the model trained for each fold. In contrast, the global analysis determines an optimal threshold across all cases for each model. The threshold in both instances is selected to maximize the balance between sensitivity and specificity, using Receiver-Operator Characteristic (ROC) Curves by maximizing Youden's Index [67], While these analyses are based on ideal thresholds applied to the test set, they serve as a guide for setting appropriate thresholds when the system is deployed in real-world applications.

In both analyses we compute segment-level classification performance metrics, specifically: Receiver-Operator Characteristic (ROC) Area Under Curve (AUC), Accuracy, Sensitivity, Specificity. For the latter three, the formulae for calculating them are:

$$\text{Accuracy} = \frac{TP + TN}{TP + TN + FP + FN}, \tag{13}$$

$$\text{Sensitivity} = \frac{TP}{TP + FN}, \tag{14}$$

$$\text{Specificity} = \frac{TN}{TN + FP}, \tag{15}$$

where TP, FP, TN, FN correspond to the number of true positive, false positive, true negative and false negative segment classifications at the given threshold. The ROC curve results from plotting the true positive rate (sensitivity) against the false positive rate ($1 - Specificity$) at various threshold settings, and AUC corresponds to the area under it, which indicates the classifier's ability to distinguish between seizure and non-seizure samples. Accuracy measures the overall correctness by the ratio of correctly classified segments, Sensitivity measures the ability to detect all seizure segments while Specificity measures the ability to avoid false detections.

In the case specific analysis, we aggregate the performance metrics across all folds, providing mean values for each one as well as the average of the selected thresholds along with its Coefficient of Variation (CoV) to demonstrate its tendency to vary across cases. In the global analysis, we report the performance scores obtained using the optimal threshold of the ROC curve resulting from the entire dataset.

Additionally, to test our model's performance as an early warning system, using the procedure we outlined for generating warnings, the following evaluation is applied: We simulate a practical deployment case by isolating a segment of pre-ictal activity (at least 1 min prior to

seizure) and train a model on a sub-sample of features generated from this segment. We then deploy the model by deriving anomaly scores that we average across a continuous 30-sample window. Using these scores, we then calculate the optimal score and time thresholds (s_c, $andt_c$) in terms of latency / lead time, using a fixed percentage of acceptable false positive duration a. We tested levels of acceptable false positive duration at 0 %, 2 %, 4 %, and 6 % of the total duration of the pre-ictal interval. We repeated this process for 50 trials in each case, bootstrapping the training set of the model deployed. For a case to be considered passable, a feasible pair of (s_c,t_c) should be capable of generating a warning within 30 s of seizure onset in at least 45 (90 %) of these trials.

3. Results

We applied the above-mentioned methodology to our clinical dataset using both modalities as well as on three different fusion schemes.

The MCD detector was parameterized using the estimated percentage of contamination samples, but it was instantiated with automatic contamination level estimation.We set the LOF computation to 200 neighbor samples. The IsF ensemble was set to 200 tree classifiers. The OCSVM detector was instantiated with a polynomial kernel of degree 2 and $\nu = 0.1$ setting an upper bound on the fraction of margin errors.

In our evaluation of the model's capabilities, we focused on analyzing the performance across different modality combinations, including EEG and ECG data, while employing various fusion techniques. The results, delineated in Tables 3 and 4, highlight the effectiveness of these models using both case-optimal and global thresholds. Additionally, the distribution of anomaly scores and ROC curves are presented in Fig. 4a and 4b, respectively. Note that results which pertain to the OCSVM model are included under the simplified abbreviation "SVM".

The patient-specific thresholds analysis showed that in the EEG modality, the LOF and MCD model showed the best performance with AUC of 92.85 % and 92.88 % and accuracies of 92.08 % and 91.88 %, respectively. For the ECG modality performance was overall significantly lower with the best performing model being the MCD model which led with an AUC of 86.44 % and accuracy of 89.75 % followed by the LOF with an AUC of 83.95 % and an accuracy of 88.37 %. The type of fusion technique used enhanced detection performance. Early fusion was significantly effective in enhancing detection capabilities for the models, with the LOF and IsF models showing AUCs of 95.01 % and 94.66 % respectively. Similarly, the sum fusion method also proved beneficial, yielding AUCs of up to 94.92 % for the LOF model and 94.26 % for the IsF model. The max fusion technique also showed promise, with the LOF model recording an AUC of 94.92 %. These fusion techniques also displayed potential in improving accuracy, specificity, and sensitivity. For instance, with early fusion, the IsF model exhibited an accuracy of 93.98 %, a sensitivity of 92.48 %, and a specificity of 95.37 %. Other notable performance metrics are highlighted in the table.

For global thresholds, performance metrics were significantly lower across all models compared to patient-specific thresholds. In the EEG modality, the MCD model demonstrated the most robust detection, with an AUC of 87.99 % and an accuracy of 80.20 %. For the ECG modality, the MCD model led again achieving an AUC of 84.59 % and an accuracy of 76.39 %. The fusion methods' potential was noticeable, as they managed to improve performances more significantly compared to the improvements achieved for patient-specific thresholds. Notably, MCD and LOF achieved AUCs of 90.62 % and 91.13 %, and accuracies of 82.58 % and 82.36 % respectively when using sum fusion. Similarly, the same models using the early fusion method attained AUCs of 90.83 % and 89.30 %, and accuracies of 82.73 % and 82.36 %. These fusion techniques also exhibited promise in improving other performance metrics such as sensitivity and specificity. For instance, the MCD model using min fusion achieved 87.01 % sensitivity – suffering however from low specificity 69.81 %. This score is closely followed by the IsF model using sum fusion with a sensitivity of 85.14 % and improved specificity 76.85 %.

These results suggest a need for patient-specific calibration upon deployment. This need is further demonstrated by the variability in the optimal threshold selection as can be seen by the Coefficient of Variation (CoV) in Table 3. For instance, while the LOF detector is overall highly effective, optimal threshold calibration may present difficulties in practical deployment, as optimal thresholds differ widely, with threshold CoV values of 18–62 % observed for multimodal detectors. On the other hand, the IsF model presents highly stable thresholds, with CoV not exceeding 10 % across multi-modal detectors.

For warning generation performance, we estimated average score and time threshold s_c, t_c derived by the process described in Section 2.E, aiming to optimize latency-lead time with a minimum false positive duration. In Fig. 5 we present a summary of these results, plotting the latencies for early and late warnings (light blue / red coloured

Table 3
Evaluation performance (%) on ictal / pre-ictal segment determination – Case specific optimal thresholds.

Modality	Model	AUC	Accuracy	Sensitivity	Specificity	Avg. Threshold	Threshold CoV
EEG	***IsF***	92.48	91.60	89.13	93.92	0.55	10.94
	LOF	92.85	92.08	90.46	93.07	1.69	35.78
	MCD	92.88	91.88	89.85	93.83	6.57	27.03
	SVM	91.26	90.58	87.11	94.60	9.45	8.36
ECG	***IsF***	81.93	86.50	79.62	92.04	0.65	22.79
	LOF	83.95	88.37	81.63	94.34	1.79	78.38
	MCD	86.44	89.75	86.57	92.72	8.26	29.92
	SVM	74.32	82.05	73.07	91.50	9.17	10.09
Fused Early	***IsF***	**94.66**	**93.98**	92.48	95.37	0.56	**9.14**
	LOF	**95.01**	**94.36**	**92.68**	**96.07**	1.79	41.88
	MCD	92.97	93.18	92.46	94.36	8.67	35.81
	SVM	92.10	91.83	88.99	96.51	10.68	6.64
Fused Late Sum	***IsF***	**94.26**	**94.10**	92.23	94.85	0.56	**9.59**
	LOF	**94.92**	**94.08**	**92.52**	**95.63**	1.7	44.65
	MCD	93.73	93.92	92.45	95.29	7.3	24.16
	SVM	92.09	91.49	87.80	96.18	9.16	6.82
Fused Late Min	***IsF***	91.86	91.40	89.43	93.03	0.52	**9.27**
	LOF	89.11	89.05	87.24	91.84	1.22	18.07
	MCD	92.89	92.04	89.87	94.05	5.99	15.71
	SVM	84.63	85.04	82.75	90.08	8.5	8.31
Fused Late Max	***IsF***	92.08	93.36	88.81	**97.05**	0.62	**7.33**
	LOF	94.36	93.86	92.51	95.26	2.21	61.86
	MCD	90.70	92.54	90.23	94.99	8.81	29.53
	SVM	84.63	85.04	82.75	90.08	8.5	8.31

Table 4
Evaluation performance (%) on ictal / pre-ictal segment determination – Global Thresholds.

Modality	Model	AUC	Accuracy	Sensitivity	Specificity	Threshold
EEG	***IsF***	80.65	74.75	59.66	89.54	0.49
	LOF	87.98	79.50	76.70	82.25	1.14
	MCD	87.99	80.20	77.81	82.55	5.09
	SVM	77.91	74.67	57.21	91.77	9.05
ECG	***IsF***	83.02	76.17	69.13	83.07	0.57
	LOF	81.36	75.14	68.13	82.01	1.23
	MCD	84.59	76.39	79.38	73.53	6.93
	SVM	61.46	61.74	33.57	89.35	9.38
Fused Early	***IsF***	88.18	78.98	82.21	75.81	0.49
	LOF	**89.62**	**81.61**	79.26	83.91	1.16
	MCD	**90.26**	**82.63**	**85.67**	79.66	7.02
	SVM	74.76	73.94	57.78	89.77	10.28
Fused Late Sum	***IsF***	**89.58**	**81.00**	**85.14**	76.95	0.5
	LOF	**91.13**	**82.73**	81.42	84.01	1.2
	MCD	**90.62**	**82.36**	79.66	85.00	6.5
	SVM	76.42	73.60	55.81	91.04	8.95
Fused Late Min	***IsF***	**89.09**	**81.59**	76.16	**86.92**	0.58
	LOF	**89.98**	**81.80**	81.97	81.64	1.3
	MCD	88.07	78.64	**87.66**	69.81	6.94
	SVM	70.33	68.01	47.13	88.48	8.47
Fused Late Max	***IsF***	80.34	74.76	60.40	88.83	0.49
	LOF	86.93	80.11	77.76	82.41	1.07
	MCD	88.68	80.82	76.37	85.18	5.12
	SVM	70.33	68.01	47.13	88.48	8.47

correspondingly) across different models in the first row of the plot. Overall, the combination of modalities led to increased early detection capabilities. The fused modalities consistently led to faster warning generation by 1–8 s. In some model instances, combining modalities results in a reduction of the number of detection failures (1–2 cases for most detectors) as well as an increase of the number of cases that could be detected prior to seizure (up to 12 cases – MCD with Early Fusion). Most notably, the multi-modal MCD detector using early fusion outperformed all other detectors and it was able to successfully generate early warnings on average 16–24 s prior to seizure in all cases with a minimal false positive percentage. Finally, we note that in all cases there was a distinct trade-off between the false positive duration and warning timeliness. Generally, increasing the threshold of the acceptable false positive percentage led to more timely warnings, as indicated by the trend observed in Fig. 5.

4. Discussion

In our evaluation of the anomaly detection applied to the pediatric focal epilepsy dataset, the performance variation across various anomaly detectors and fusion techniques was made evident. While the overall detection performance metrics exhibited slight improvement when considering modality fusion over the EEG modality alone, the true benefit of exploiting the ECG was made clear when evaluating warning generation timeliness. Modality fusion, particularly early fusion, yielded notable improvement in early seizure detection. Most notably, the multimodal MCD produced early warnings in all cases.

We compare our performance results with three other related studies in the literature by Greene et al. [68], Vandecasteele et al. [15] and Mesbah et al. [14]. The comparison of different methods for seizure prediction and detection is challenging due to varying configuration factors in different experiments. These factors include different evaluation metrics, the number of seizures and patients involved, the timing of the prediction, and whether the models are trained patient-specific or in-specific manner. These studies were selected for their approach and performance measures utilized, which are similar to ours, although they were conducted on different datasets. It is important to also note that the work of Greene et al. and Mesbah et al. was conducted on data of neonatal patients, a population that poses similar attributes with our dataset. Our patient-specific system with case-optimized thresholds achieved significantly higher scores than those reported in the two first studies, and comparable results with those of Mesbah, all while our models do not require labeled seizure samples to train. Utilizing unimodal EEG models we reached an AUC of 93 %, accuracy of 92 %, sensitivity of 90 %, and specificity of 95 %, while with the unimodal ECG models we attained scores of 86 % AUC, 90 % accuracy, 87 % sensitivity, and 94 % specificity, all of which are higher than the best scores reported by these studies. Finally, with modality fusion our scores of 93 % AUC, 94 % accuracy, 93 % sensitivity, and 97 % specificity were again notably higher, slightly surpassing Vandecasteele's model in terms of sensitivity with scores in the range 84 %-92 %, and also surpassing Mesbah in terms of specificity but falling slightly behind in sensitivity, with values 94 % and 95 % respectively. This comparison is showcased in Table 5.

When it comes to the timeliness of seizure prediction, there is significant variability in the findings of recent studies, primarily attributed to the diverse methodologies employed for generating seizure warnings [67]. Our work shows significant similarity in prediction performance when compared to the study [39] in which a detection framework that achieved an prediction time of 21.8 s was presented. Other EEG-based approaches in the literature report comparable with our results, but varying, with prediction times of 6–30 s for both animal and human subjects [70,71,72,73].

As significant as the improvements our model introduces are, our models still face challenges regarding variations in optimal patient-specific threshold setting. Overall, careful threshold calibration may be vital for accurate detection, as patient-specific thresholds outperformed the global thresholds across all metrics. The trade-off between early or low latency detection and false warning generation is prevalent in the simulations we run, and it's up to clinical users to define their preferred system performance (either high latency with low false positive duration or high false positive duration with low latency). Additionally, different models appear to perform better in different configurations, with the exploitation of both modalities leading to varying improvement across performance metrics, which underlines the need for further customization upon deployment. These limitations imply that in practical settings, case-specific customization is vital prior to deployment of this framework.

A limitation of our study is the medium size dataset of 29 cases. It should be noted however that studies using datasets with a small number of cases and patients are common in related literature [11].This is in part due to the fact that our study focused only on pediatric patients,

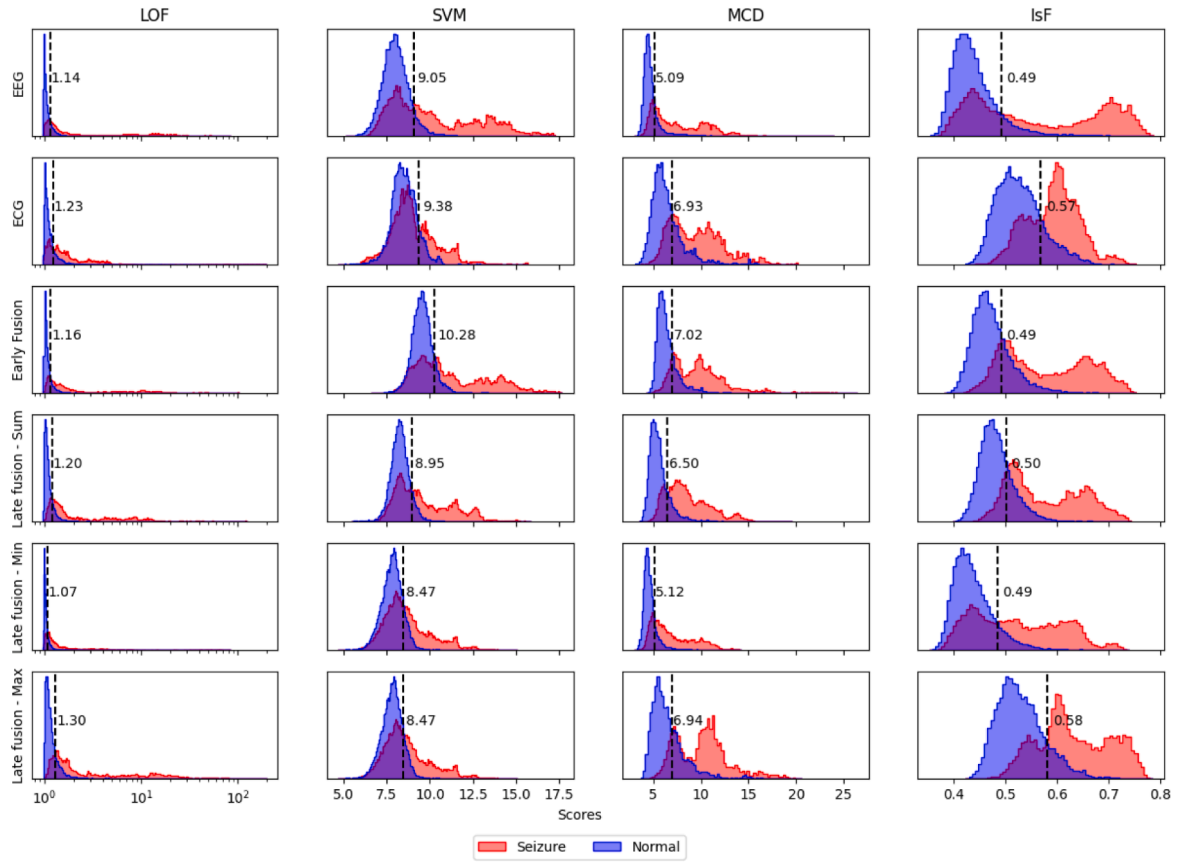

(a)

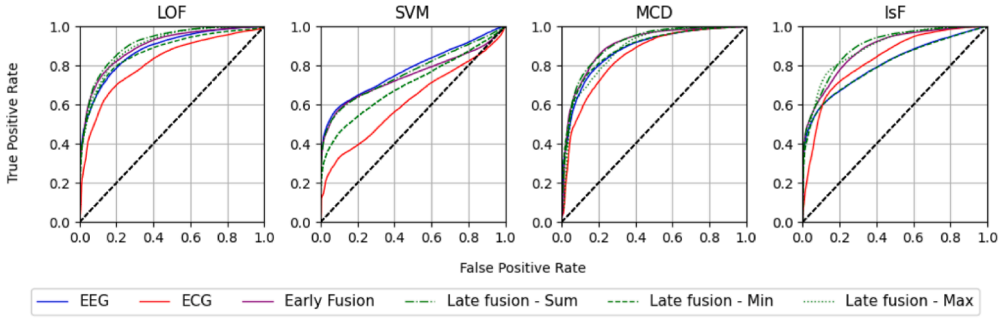

(b)

Fig. 4. Distribution histograms of anomaly scores originating from different models and different modalities / modality combinations (a) and their corresponding ROC curves (b). In (a) the red histograms correspond to anomaly scores assigned to EEG/HRV activity during seizure occurrence whereas blue histograms correspond to scores assigned to datapoints originating from normal EEG/HRV activity, the dashed lines indicate the Youden's index optimal thresholds set for the total of the dataset samples, with their value indicated on the right. In (b) the ROC curves obtained from each model for different thresholds are displayed with multiple modality combinations plotted with different colors / line styles (see legend on the right). The AUCs of these ROC curves are mentioned in Table III.

which introduces difficulties in sample collection. Additionally, our dataset contains only frontal lobe focal epilepsy cases. This limitation, however, allowed us to establish a consistent electrode configuration across cases, centered near the focus, which is in line with our pursuit of a framework ideal to a more lightweight wearable configuration.

Future research should investigate alternative or well-established state-of-the-art model architectures and diverse modalities to potentially achieve higher performance, complemented by an exhaustive optimization of hyperparameters which may yield further performance gains. Expanding the seizure detection pipeline beyond the EEG and ECG modalities to incorporate diverse sources such as accelerometry [74,75], electromyography [76], electrodermal response [77], near-infrared spectroscopy [78], photoplethysmography [79], video [80] etc. could provide comprehensive monitoring and detection of seizure-related abnormal events. Furthermore, in this study, we focused on predicting seizure onset using a small segment of EEG and ECG data, only ten minutes prior to seizure, whereas other studies have demonstrated potential for long-term predictability of seizures from EEG and ECG. These potential needs to also be explored with our proposed models, towards a fully functional early warning system.

5. Conclusion

Our study validates the effectiveness of our proposed semi-

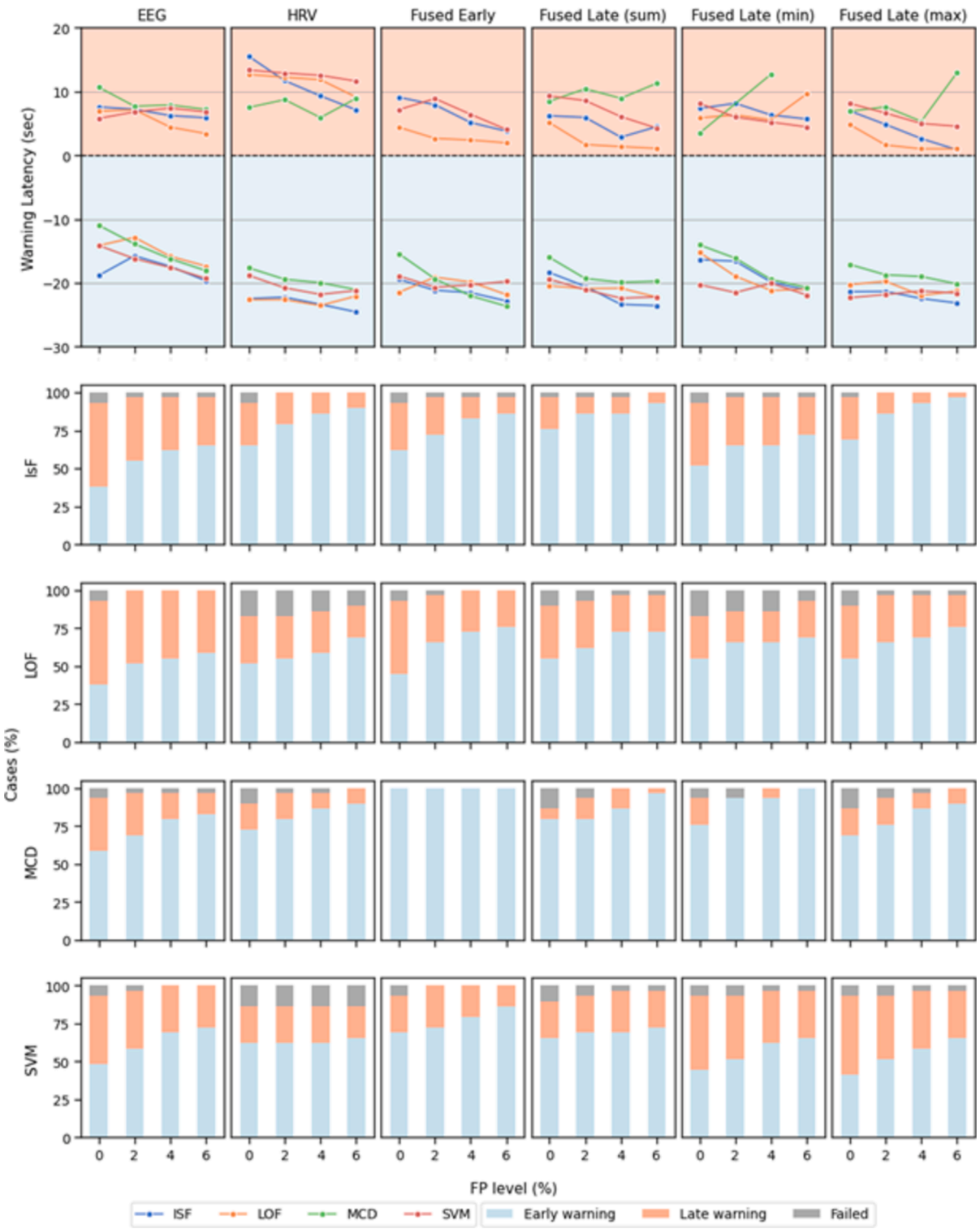

Fig. 5. Model deployment simulation trial results. Top plots visualize the average warning latency for each model across all cases, at different levels of accepted false positive percentages (x-axis). Cases are grouped based on whether our system achieved generating for them an early warning prior to seizure onset (light blue) or a late warning after the onset (light red). The stacked bar plots bellow similarly indicate the percentage (%) at which the models produced warnings prior (light blue) or after (light red) seizure onset or failed to produce warnings (gray) given the specified FP tolerance level (%).

supervised ECG / EEG method for seizure detection and prediction utilizing common anomaly detection models. The combination of these modalities notably boosts our system's early warning capabilities. It furthermore demonstrates how patient specific anomaly detection models can be easily established using normal EEG/ECG activity data from individual patients. The balance between warning latency and false warnings emerged as a crucial concern in warning threshold setting. Given epilepsy's variable nature, a flexible system that allows for parameter adjustments is vital. As sensor technology advances, the integration of EEG and ECG (HRV) monitoring into affordable wearables holds significant promise, paving the way for improved quality of life and personalized seizure management tools for pediatric individuals

Table 5
Comparison of performances (%) of literature related to seizure anomaly detection.

			EEG				*ECG*				*Fusion*			
Publication	***System Type***	***Dataset***	***AUC***	***Acc***	***Sen***	***Spe***	***AUC***	***Acc***	***Sen***	***Spe***	***AUC***	***Acc***	***Sen***	***Spe***
Vandercasteele (2023)	*Patient Specific*	*SeizeIT1*	–	–	81	–	–	–	65	–	–	–	92	–
	Supervised	*Epilepsiae Freiburg*	–	–	82	–	–	–	74	–	–	–	90	–
		Epilepsiae Paris	–	–	84	–	–	–	52	–	–	–	84	–
Mesbah (2012)	*Patient Inspecific* *Supervised*	*Royal Brisbane*	–	–	81	87	–	–	86	85	–	–	95	94
Greene(2007)	*Patient Inspecific* *Supervised*	*Kings College*	76	85	71	69	68	64	70	62	77	72	72	71
	Patient Specific *Supervised*		–	85	–	62	–	69	60	69	–	86	76	89
This study	*Patient Specific* *(Case optimized thresholds)* *Semi-supervised*	*Heraklion*	93	92	90	95	86	90	87	94	95	94	93	97
	Patient Inspecific *(Global thresholds)* *Semi-supervised*		88	80	80	92	84	85	80	90	90	83	87	92

with epilepsy.

CRediT authorship contribution statement

Apostolos Karasmanoglou: Writing – review & editing, Writing – original draft, Visualization, Validation, Software, Methodology, Investigation, Formal analysis, Conceptualization. **Giorgos Giannakakis:** Writing – review & editing, Supervision, Data curation, Conceptualization. **Pelagia Vorgia:** Writing – review & editing, Validation, Data curation. **Marios Antonakakis:** Writing – review & editing, Validation, Supervision, Project administration, Funding acquisition, Conceptualization. **Michalis Zervakis:** Writing – review & editing, Validation, Supervision, Resources, Project administration, Funding acquisition.

Declaration of competing interest

The authors declare that they have no known competing financial interests or personal relationships that could have appeared to influence the work reported in this paper.

Acknowledgment

This work was supported by the EU co-funded project 'smartHEALTH' (Digital Europe Programme (Grant Agreement No. 101083630 and the Operational Programme "Competitiveness 2021-2027" (MIS 6001551).

Appendix A

We provide a more detailed description of its mathematical formulations for each anomaly detection model we utilized.

Minimum Covariance Determinant (MCD) supposes that the inlier samples follow a multivariate Normal distribution localized about the mean $\boldsymbol{\mu}$ and covariance matrix Σ: $X_{inliers} \sim N(\boldsymbol{\mu}, \Sigma)$. Given this assumption, the Elliptic Envelope models the Mahalanobis distance D_M of each data point $\boldsymbol{x}$ from the center $\boldsymbol{\mu}$ as follows:

$$D_M(\boldsymbol{x}) = \sqrt{(\boldsymbol{x}-\boldsymbol{\mu})^T \Sigma^{-1} (\boldsymbol{x}-\boldsymbol{\mu})}. \tag{A.1}$$

However, we found that a more numerically manageable score is possible if we set the score to the log of the robust distance:

$$s(\boldsymbol{x}) = \log\left[\sqrt{(\boldsymbol{x}-\boldsymbol{\mu})^T \Sigma^{-1} (\boldsymbol{x}-\boldsymbol{\mu})}\right]. \tag{A.2}$$

The algorithm estimates the parameters of an ellipse that best fits the inliers in the feature space. Given a dataset of n observations in feature space, the MCD estimator seeks to find h observations $h < n$ that minimize the determinant of the sample covariance matrix. Any data point outside this ellipse is considered an anomaly.

The Isolation Forest (IsF) model leverages the concept of anomaly isolation through a sequence of vertical or horizontal 'splits' generated by an ensemble of decision trees. Intuitively, IsF isolates anomalies quickly because anomalies typically require fewer splits to be separated from the rest of the data. Thus, the anomaly score $s(\boldsymbol{x})$ of a data point $\boldsymbol{x}$ from a dataset of n points:

$$s(\boldsymbol{x}) = 2^{-\frac{E[h(\boldsymbol{x})]}{c(n)}}, \tag{A.3}$$

where $E[h(\boldsymbol{x})]$ is the average search path length of the data point $\boldsymbol{x}$ in the IsF and $c(n)$ is the average search path length of an unsuccessful search. It is evident from this formulation that the anomaly score takes values in the range $(0, 1]$, with 0 indicating low likelihood of anomaly, corresponding to longer average split paths and 1 indicating high likelihood of anomaly, corresponding to shorter average split paths.

SVM models generally aim to find a hyperplane that separates inliers from the origin in a high-dimensional space. In the One-Class instance of the SVM model (OCSVM), we aim to estimate the minimum volume estimator of classes boundary, i.e., the decision function of a OCSMV is:

$$f(\boldsymbol{x}) = sign(\langle \boldsymbol{w}, \phi(\boldsymbol{x}) \rangle - \rho), \tag{A.4}$$

where $\boldsymbol{w}$ is a parameter vector $\phi(\boldsymbol{x}) : \mathbb{R}^N \rightarrow \mathbb{R}^d$ is a feature mapping and ρ is a radius parameter that controls the volume of the classification boundary bounding the inlier set. The choice of kernel function (e.g., linear, polynomial, radial basis function) determines the feature mapping $\phi : X \rightarrow V$ and affects the shape of the decision boundary. In order to score feature vectors, we utilize the following modification of the decision function derive

an anomaly score:

$$s(\boldsymbol{x}) = R(\langle \boldsymbol{w}, \phi(\boldsymbol{x}) \rangle - \rho), \tag{A.5}$$

where $R(.)$ is a ramp function.

LOF (Local Outlier Factor) is a distance-based anomaly detection technique that evaluates the local density of data points, identifying outliers residing in sparsely populated regions. LOF quantifies density by calculating the reachability distance between data points based on their k-nearest neighbors. It distinguishes between inliers, which typically lie within densely populated regions ensuring a minimum distance bound. The Local Reachability Density (LRD) metric quantifies the neighborhood's density by averaging the reachability distances of a data point's neighbors. Reachability distance between two points $\boldsymbol{x}_i, \boldsymbol{x}_j$ in feature space is defined as:

$$rd_k(\boldsymbol{x}_i, \boldsymbol{x}_j) = max\{d(x_j, n_k(\boldsymbol{x}_j)), d(\boldsymbol{x}_i, \boldsymbol{x}j)\}, \tag{A.6}$$

where $d(.)$ is the distance metric, usually Euclidian distance, and $n_k(\boldsymbol{x}_j)$ is the k-th nearest neighbor of the point $\boldsymbol{x}_j$. Based on this, the local reachability distance is defined as:

$$lrd(\boldsymbol{x}_i, k) = \left(\frac{1}{k} \sum_{j=1}^{k} rd(\boldsymbol{x}_i, n_j(\boldsymbol{x}_i)) \right)^{-1}. \tag{A.7}$$

The LOF itself is calculated as the average ratio between a point's LRD and that of its k nearest neighbors:

$$LOF(\boldsymbol{x}_i, k) = \frac{1}{k} \sum_{j=1}^{k} \frac{lrd(\boldsymbol{x}_i, k)}{lrd(n_j(\boldsymbol{x}_i, j), k)}, \tag{A.8}$$

values less than one suggest increased density compared to neighbors, while values greater than one indicates lower local density, signifying outlier behavior. LOF is used directly as the anomaly score:

$$s(\boldsymbol{x}) = LOF(\boldsymbol{x}, k) \tag{A.9}$$

Appendix B

In the following, we include supplementary information regarding the capabilities of the warning generation methodology we proposed using the different models we investigated in the study. Bellow we list the number of cases in which we were able to generate early warnings (prior to seizure), late warnings (after seizure onset), grouped by modality / modality fusion methodology and acceptable false positive percentage – α (See sections 2.F, 2.G), we list the average score and time thresholds s_c, t_c as indicators of how such a value could be set in deployment, as well as the average latency in case of late warning, or lead-time in case of early warning ΔT_L, and false warning duration ΔT_{FW} measured in seconds.

Modality	Model	Early warning						Late warning					Failed
		α	s_c	t_c	ΔT_L	ΔT_{FW}	# Cases	s_c	t_c	ΔT_L	ΔT_{FW}	# Cases	
EEG	***IsF***	**0 %**	0.5	11.25	−18.85	0.0	11	0.5	2.75	7.58	0.0	16	2
		2 %	0.49	8.49	−15.77	4.36	16	0.5	1.68	7.22	4.62	12	1
		4 %	0.48	7.46	−17.42	9.47	18	0.49	0.45	6.23	7.76	10	1
		6 %	0.47	7.34	−19.69	13.93	19	0.48	0.01	5.88	8.23	9	1
	LOF	**0 %**	1.21	3.55	−14.15	0.0	11	1.18	3.05	6.92	0.0	16	2
		2 %	1.2	5.49	−12.88	2.68	15	1.15	2.11	7.14	2.92	14	0
		4 %	1.13	6.34	−15.85	7.04	16	1.13	1.83	4.41	4.76	13	0
		6 %	1.12	6.28	−17.39	10.44	17	1.13	1.43	3.4	6.46	12	0
	MCD	**0 %**	5.41	9.94	−10.98	0.0	17	5.95	8.15	10.66	0.0	10	2
		2 %	5.36	9.31	−13.9	5.1	20	5.88	8.26	7.7	6.58	8	1
		4 %	5.32	8.77	−16.23	11.02	23	5.63	6.39	7.9	12.74	5	1
		6 %	5.28	7.99	−18.09	16.0	24	5.59	6.08	7.2	18.29	4	1
	SVM	**0 %**	7.11	5.96	−14.14	0.0	14	7.54	1.99	5.77	0.0	13	2
		2 %	7.08	5.61	−16.22	3.49	17	7.42	2.73	6.8	3.42	11	1
		4 %	7.08	5.57	−17.58	7.59	20	7.37	1.83	7.4	4.75	9	0
		6 %	7.05	6.3	−19.31	10.07	21	7.34	1.7	6.8	6.6	8	0
HRV	***IsF***	**0 %**	0.54	7.82	−22.47	0.0	19	0.55	13.17	15.5	0.0	8	2
		2 %	0.54	8.37	−22.25	4.26	23	0.54	11.35	11.7	5.98	6	0
		4 %	0.53	7.5	−23.38	8.59	25	0.54	12.11	9.31	9.94	4	0
		6 %	0.53	6.92	−24.57	11.79	26	0.54	13.77	7.11	16.37	3	0
	LOF	**0 %**	1.13	5.66	−22.64	0.0	15	1.24	0.37	12.67	0.0	9	5
		2 %	1.19	5.25	−22.64	1.74	16	1.08	1.15	12.23	1.35	8	5
		4 %	1.17	6.15	−23.55	4.52	17	1.06	3.84	11.85	4.53	8	4
		6 %	1.15	5.73	−22.08	9.15	20	1.05	4.37	9.11	5.79	6	3
	MCD	**0 %**	7.01	7.67	−17.67	0.0	21	7.66	10.24	7.51	0.0	5	3
		2 %	6.82	7.63	−19.45	4.37	23	7.79	9.26	8.72	5.15	5	1
		4 %	6.8	7.28	−19.98	8.42	25	6.75	13.45	5.91	14.81	3	1
		6 %	6.69	7.1	−21.07	12.28	26	6.27	16.46	8.93	25.26	3	0
	SVM	**0 %**	7.5	4.65	−18.85	0.0	18	7.16	0.08	13.36	0.0	7	4
		2 %	7.47	4.88	−20.79	1.96	18	7.15	0.2	12.89	1.02	7	4
		4 %	7.46	4.89	−21.82	4.41	18	7.14	0.35	12.54	2.47	7	4

(continued on next page)

(*continued*)

Modality	Model	Early warning						Late warning					Failed
		α	s_c	t_c	ΔT_L	ΔT_{FW}	# Cases	s_c	t_c	ΔT_L	ΔT_{FW}	# Cases	
		6 %	7.4	4.57	−21.2	6.16	19	7.24	1.93	11.63	7.81	6	4
Early Fused	***IsF***	**0 %**	0.51	8.57	−19.46	0.0	18	0.53	7.38	9.09	0.0	9	2
		2 %	0.5	8.86	−21.17	4.49	21	0.51	7.6	7.92	4.86	7	1
		4 %	0.5	8.88	−21.54	8.77	24	0.51	6.99	5.13	6.89	4	1
		6 %	0.49	9.9	−22.85	12.31	25	0.52	3.14	3.79	4.65	3	1
	LOF	**0 %**	1.15	7.03	−21.47	0.0	13	1.15	3.91	4.38	0.0	14	2
		2 %	1.12	7.88	−19.11	4.04	19	1.13	3.3	2.65	1.98	9	1
		4 %	1.1	7.56	−19.87	7.9	21	1.15	2.84	2.4	3.18	8	0
		6 %	1.09	7.85	−21.85	12.25	22	1.15	0.89	1.95	2.33	7	0
	MCD	**0 %**	7.14	7.58	−15.46	0.0	29					0	0
		2 %	6.95	6.47	−19.38	5.41	29					0	0
		4 %	6.78	5.89	−22.05	10.41	29					0	0
		6 %	6.67	5.75	−23.66	14.43	29					0	0
	SVM	**0 %**	8.64	6.9	−18.94	0.0	20	8.62	1.84	7.17	0.0	7	2
		2 %	8.59	6.57	−20.69	3.0	21	8.77	3.66	8.89	3.14	8	0
		4 %	8.64	5.8	−20.32	6.02	23	8.63	4.95	6.41	5.44	6	0
		6 %	8.6	5.89	−19.78	7.87	25	8.85	5.73	4.05	11.89	4	0

Modality	Model	Early warning						Late warning					Failed
		α	s_c	t_c	ΔT_L	ΔT_{FW}	# Cases	s_c	t_c	ΔT_L	ΔT_{FW}	# Cases	
Late Fused Sum	***IsF***	**0 %**	0.5	11.56	−18.38	0.0	22	0.52	7.75	6.2	0.0	6	1
		2 %	0.5	9.91	−20.55	4.83	25	0.51	9.99	5.94	4.95	3	1
		4 %	0.5	8.76	−23.37	8.79	25	0.51	10.16	2.84	9.89	3	1
		6 %	0.49	8.88	−23.57	12.42	27	0.5	13.34	4.47	18.06	2	0
	LOF	**0 %**	1.17	6.0	−20.48	0.0	16	1.09	2.96	5.12	0.0	10	3
		2 %	1.15	7.85	−20.9	3.31	18	1.08	3.64	1.69	2.4	9	2
		4 %	1.13	8.3	−20.84	8.27	21	1.05	0.25	1.36	0.99	7	1
		6 %	1.12	7.57	−22.25	11.58	21	1.05	0.11	1.09	1.53	7	1
	MCD	**0 %**	6.08	7.48	−16.0	0.0	23	6.53	8.45	8.47	0.0	2	4
		2 %	5.93	7.37	−19.32	4.45	23	6.37	12.99	10.41	6.58	4	2
		4 %	5.87	7.38	−19.93	8.72	25	6.37	16.07	8.94	15.59	4	0
		6 %	5.87	7.58	−19.75	13.64	28	5.81	16.7	11.28	26.36	1	0
	SVM	**0 %**	7.28	7.5	−19.43	0.0	19	7.3	1.41	9.29	0.0	7	3
		2 %	7.29	7.09	−21.06	2.82	20	7.31	1.66	8.58	2.67	7	2
		4 %	7.28	6.78	−22.41	5.03	20	7.36	4.28	6.06	7.43	8	1
		6 %	7.25	6.68	−22.2	6.87	21	7.42	2.53	4.26	11.38	7	1
Late Fused Min	***IsF***	**0 %**	0.48	8.76	−16.36	0.0	15	0.48	3.64	7.36	0.0	12	2
		2 %	0.47	6.85	−16.61	4.5	19	0.48	2.44	8.15	4.4	9	1
		4 %	0.47	5.12	−19.88	8.44	19	0.47	2.1	6.32	8.37	9	1
		6 %	0.46	6.43	−21.15	12.51	21	0.47	0.12	5.69	10.78	7	1
	LOF	**0 %**	1.03	4.88	−15.24	0.0	16	1.03	4.25	5.86	0.0	8	5
		2 %	1.03	7.27	−18.96	3.78	19	1.02	0.54	6.32	3.06	6	4
		4 %	1.03	6.93	−21.19	6.89	19	1.02	0.86	5.54	5.29	6	4
		6 %	1.02	7.68	−20.99	9.67	20	1.01	4.83	9.64	9.4	7	2
	MCD	**0 %**	5.08	9.78	−14.06	0.0	22	5.2	14.35	3.47	0.0	5	2
		2 %	5.01	9.07	−16.14	5.79	27					0	2
		4 %	4.96	7.59	−19.49	11.12	27	5.66	14.31	12.71	17.61	2	0
		6 %	4.96	7.5	−20.74	16.29	29					0	0
	SVM	**0 %**	6.78	5.98	−20.29	0.0	13	6.84	3.24	8.15	0.0	14	2
		2 %	6.82	6.78	−21.52	3.01	15	6.75	2.38	5.98	2.94	12	2
		4 %	6.82	6.96	−20.07	6.42	18	6.75	2.1	5.2	4.52	10	1
		6 %	6.81	7.12	−21.92	9.11	19	6.69	2.36	4.45	6.59	9	1
Late Fused Max	***IsF***	**0 %**	0.55	8.24	−21.4	0.0	20	0.56	12.71	6.96	0.0	8	1
		2 %	0.54	8.02	−21.34	4.51	25	0.55	13.66	4.83	6.16	4	0
		4 %	0.54	7.16	−22.46	8.94	27	0.57	9.68	2.62	7.12	2	0
		6 %	0.54	6.82	−23.17	12.13	28	0.55	14.2	0.85	9.19	1	0
	LOF	**0 %**	1.3	5.83	−20.27	0.0	16	1.18	2.86	4.82	0.0	10	3
		2 %	1.26	7.54	−19.76	3.58	19	1.1	3.9	1.61	2.29	9	1
		4 %	1.21	7.95	−21.98	8.02	20	1.09	2.78	1.01	3.04	8	1
		6 %	1.19	7.43	−21.29	11.25	22	1.07	0.16	1.02	1.25	6	1
	MCD	**0 %**	7.21	6.56	−17.12	0.0	20	8.0	13.98	6.89	0.0	5	4
		2 %	6.99	7.34	−18.74	4.4	22	8.09	12.24	7.6	5.86	5	2
		4 %	7.0	7.63	−19.01	8.75	25	6.89	13.88	5.32	14.19	3	1
		6 %	6.89	7.28	−20.17	12.81	26	6.65	17.02	12.96	22.96	3	0
	SVM	**0 %**	6.75	5.25	−22.34	0.0	12	6.89	3.49	8.13	0.0	15	2
		2 %	6.82	6.36	−21.84	2.97	15	6.77	2.29	6.62	2.97	12	2
		4 %	6.84	6.92	−21.27	6.06	17	6.75	2.55	4.99	5.33	11	1
		6 %	6.82	6.88	−21.61	8.7	19	6.71	2.2	4.55	6.62	9	1

Data availability

The data that has been used is confidential.

References

[1] World Health Organization, 'Epilepsy'. Accessed: Dec. 02, 2022. [Online]. Available: https://www.who.int/news-room/fact-sheets/detail/epilepsy.

[2] NHS Inform, 'Epilepsy'. [Online]. Available: https://www.nhsinform.scot/illnesses-and-conditions/brain-nerves-and-spinal-cord/epilepsy/#:~:text=Epilepsy%20is%20a%20condition%20that,100%20people%20has%20the%20condition.

[3] Johns Hopkins Medicine, 'Focal Epilepsy'. [Online]. Available: https://www.hopkinsmedicine.org/health/conditions-and-diseases/epilepsy/focal-epilepsy.

[4] F.A. Chowdhury, R. Silva, B. Whatley, M.C. Walker, Localisation in focal epilepsy: a practical guide, *Pract. Neurol.* 21 (6) (2021) 481–491, https://doi.org/10.1136/practneurol-2019-002341.

[5] R. Gurney, F. Rugg-Gunn, M.K. Sidhu, 010 Seizure semiology of frontal lobe epilepsy (FLE): a report of two cases with video-telemetry recordings, *J. Neurol. Neurosurg. Psychiatry* 93 (2022) A104–A, https://doi.org/10.1136/jnnp-2022-ABN.335.

[6] P. Tinuper, F. Bisulli, From nocturnal frontal lobe epilepsy to Sleep-Related Hypermotor Epilepsy: A 35-year diagnostic challenge, *Seizure* 44 (2017) 87–92, https://doi.org/10.1016/j.seizure.2016.11.023.

[7] D. K. Starnes II, B. H. Brinkmann, and K. J. Miller, 'Pediatric epilepsy: Defining syndromes and applying innovative therapies', *Mayo Clinic*, Nov. 2021, [Online]. Available: https://www.mayoclinic.org/medical-professionals/neurology-neurosurgery/news/pediatric-epilepsy-defining-syndromes-and-applying-innovative-therapies/mac-20431121.

[8] Children's Hospital of Philadelphia, 'Focal Epilepsy in Children'. [Online]. Available: https://www.chop.edu/conditions-diseases/focal-epilepsy-children.

[9] H. O. Lüders, Ed., *Epilepsy Surgery*, 2nd ed. Boca Raton: CRC Press, 2008.

[10] J.S. Ebersole, A.M. Husain, *The Clinical EEG Handbook*, Demos Medical Publishing, New York, 2003.

[11] M.K. Siddiqui, R. Morales-Menendez, X. Huang, N. Hussain, A review of epileptic seizure detection using machine learning classifiers, *Brain Inf.* 7 (1) (2020) Dec, https://doi.org/10.1186/s40708-020-00105-1.

[12] F. Mason *et al.*, 'Heart Rate Variability as a Tool for Seizure Prediction: A Scoping Review', *Journal of Clinical Medicine*, vol. 13, no. 3, Art. no. 3, Jan. 2024, doi: 10.3390/jcm13030747.

[13] M. Qaraqe, M. Ismail, E. Serpedin, H. Zulfi, Epileptic seizure onset detection based on EEG and ECG data fusion, *Epilepsy Behav.* 58 (2016) 48–60, https://doi.org/10.1016/j.yebeh.2016.02.039.

[14] M. Mesbah, M. Balakrishnan, P.B. Colditz, B. Boashash, Automatic seizure detection based on the combination of newborn multi-channel EEG and HRV information, *EURASIP Journal on Advances in Signal Processing* 2012 (1) (2012) 215, https://doi.org/10.1186/1687-6180-2012-215.

[15] K. Vandecasteele, et al., The power of ECG in multimodal patient-specific seizure monitoring: Added value to an EEG-based detector using limited channels, *Epilepsia* 62 (10) (2021) 2333–2343, https://doi.org/10.1111/epi.16990.

[16] G.M. Sigsgaard, Y. Gu, Comparison of patient non-specific seizure detection using multi-modal signals, *Neurosci. Inf.* 4 (1) (2024) 100152, https://doi.org/10.1016/j.neuri.2023.100152.

[17] A. van Westrhenen, T. De Cooman, R.H.C. Lazeron, S. Van Huffel, R.D. Thijs, Ictal Autonomic Changes as a Tool for Seizure Detection: A Systematic Review, *Clin Auton Res* 29 (2) (2019) 161–181, https://doi.org/10.1007/s10286-018-0568-1.

[18] L. Mazzola, S. Rheims, Ictal and Interictal Cardiac Manifestations in Epilepsy. A Review of Their Relation With an Altered Central Control of Autonomic Functions and With the Risk of SUDEP, *Front. Neurol.* 12 (2021).

[19] J.W. Britton, G.R. Ghearing, E.E. Benarroch, G.D. Cascino, The Ictal Bradycardia Syndrome: Localization and Lateralization, *Epilepsia* 47 (4) (2006) 737–744, https://doi.org/10.1111/j.1528-1167.2006.00509.x.

[20] S. Behbahani, N.J. Dabanloo, A.M. Nasrabadi, C.A. Teixeira, A. Dourado, Pre-ictal Heart Rate Variability Assessment of Epileptic Seizures by Means of Linear and Non-linear Analyses, *Anadolu Kardiyol Derg* 13 (8) (2013) 797–803, https://doi.org/10.5152/akd.2013.237.

[21] R. Pernice, et al., Time, Frequency and Information Domain Analysis of Short-term Heart Rate Variability Before and After Focal and Generalized Seizures in Epileptic Children, *Physiol Meas* 40 (7) (2019) 074003, https://doi.org/10.1088/1361-6579/ab16a3.

[22] S.J. van der Kruijs, et al., Autonomic Nervous System Functioning Associated with Psychogenic Nonepileptic Seizures: Analysis of Heart Rate Variability, *Epilepsy Behav* 54 (2016) 14–19, https://doi.org/10.1016/j.yebeh.2015.10.014.

[23] F. Leutmezer, C. Schernthaner, S. Lurger, K. Pötzelberger, C. Baumgartner, Electrocardiographic Changes at the Onset of Epileptic Seizures, *Epilepsia* 44 (3) (2003) 348–354, https://doi.org/10.1046/j.1528-1157.2003.34702.x.

[24] W. Tatum, How not to read an EEG, *Neurology* 80 (2013) S1–S3, https://doi.org/10.1212/WNL.0b013e318279730e.

[25] N. Gaspard, L. Hirsch, Pitfalls in ictal EEG interpretation, *Neurology* 80 (2013) S26–S42, https://doi.org/10.1212/WNL.0b013e31827974f8.

[26] D. Popivanov, A. Mineva, Testing procedures for non-stationarity and non-linearity in physiological signals, *Math. Biosci.* 157 (1–2) (1999) 303–320, https://doi.org/10.1016/S0025-5564(98)10088-3.

[27] M. Signorini, S. Cerutti, S. Guzzetti, R. Parola, Non-Linear Dynamics of Cardiovascular Variability Signals, *Methods Inf. Med.* 33 (1994) 81–84, https://doi.org/10.1055/s-0038-1634981.

[28] D. Smit, D. Boomsma, H. Schnack, H.H.H. Pol, E.D. de Geus, Individual Differences in EEG Spectral Power Reflect Genetic Variance in Gray and White Matter Volumes, *Twin Res. Hum. Genet.* 15 (2012) 384–392, https://doi.org/10.1017/thg.2012.6.

[29] J.K. Kanters, M. Højgaard, E. Agner, N. Holstein-Rathlou, Short- and long-term variations in non-linear dynamics of heart rate variability, *Cardiovasc. Res.* 31 (3) (1996) 400–409, https://doi.org/10.1016/S0008-6363(95)00085-2.

[30] M.E. Villa-Pérez, M.Á. Álvarez-Carmona, O. Loyola-González, M.A. Medina-Pérez, J.C. Velazco-Rossell, K.-K.-R. Choo, Semi-supervised anomaly detection algorithms: A comparative summary and future research directions, *Knowl.-Based Syst.* 218 (2021) 106878, https://doi.org/10.1016/j.knosys.2021.106878.

[31] O. Chapelle, B. Schoelkopf, and A. Zien, Eds., *Semi-Supervised Learning*. in Adaptive Computation and Machine Learning Series. London, England: MIT Press, 2019.

[32] C. Maher, Y. Yang, N. D. Truong, C. Wang, A. Nikpour, and O. Kavehei, 'Seizure detection with reduced electroencephalogram channels: research trends and outlook', *R Soc Open Sci*, vol. 10, no. 5, p. 230022, doi: 10.1098/rsos.230022.

[33] D. Sopic, A. Aminifar, and D. Atienza, 'e-Glass: A Wearable System for Real-Time Detection of Epileptic Seizures', May 2018, pp. 1–5. doi: 10.1109/ISCAS.2018.8351728.

[34] J. Prasanna, M.S.P. Subathra, M.A. Mohammed, R. Damaševičius, N.J. Sairamya, S. T. George, Automated Epileptic Seizure Detection in Pediatric Subjects of CHB-MIT EEG Database-A Survey, *J Pers Med* 11 (10) (Oct. 2021) 1028, https://doi.org/10.3390/jpm11101028.

[35] T. Sonmezocak, G. Guler, M. Yildiz, Classification of Resampled Pediatric Epilepsy EEG Data Using Artificial Neural Networks with Discrete Fourier Transforms, *Elektronika Ir Elektrotechnika* (2023), https://doi.org/10.5755/j02.eie.34433.

[36] V.A. Vakorin, et al., Exploring Age-Related Changes in Dynamical Non-Stationarity in Electroencephalographic Signals during Early Adolescence, *PLoS One* 8 (2013), https://doi.org/10.1371/journal.pone.0057217.

[37] A. Kaminska, F. Chéliout-Héraut, M. Eisermann, A.T. Villepin, M. Lamblin, EEG in children, in the laboratory or at the patient's bedside, *Neurophysiologie Clinique/clinical Neurophysiology* 45 (2015) 65–74, https://doi.org/10.1016/j.neucli.2014.11.008.

[38] G. Giannakakis, N. Tsekos, K. Giannakaki, K. Michalopoulos, P. Vorgia, M. Zervakis, *Seizure Detection Using Common Spatial Patterns and Classification Techniques*. (2019), https://doi.org/10.1109/BIBE.2019.00166.

[39] G. Giannakakis, M. Tsiknakis, and P. Vorgia, 'Focal epileptic seizures anticipation based on patterns of heart rate variability parameters', *Computer Methods and Programs in Biomedicine*, pp. 123–133, 2019.

[40] D. Nabil and F. Bereksi Reguig, 'Ectopic beats detection and correction methods: A review', *Biomedical Signal Processing and Control*, vol. 18, pp. 228–244, Apr. 2015, doi: 10.1016/j.bspc.2015.01.008.

[41] K. A. Myers, S. Sivathamboo, and P. Perucca, 'Heart rate variability measurement in epilepsy: How can we move from research to clinical practice?', *Epilepsia*, vol. 59, no. 12. Wiley Periodicals, Inc., pp. 2169–2178, 2018. doi: 10.1111/epi.14587.

[42] V. Toth *et al.*, 'Periictal heart rate variability analysis suggests long-term postictal autonomic disturbance in epilepsy', *European Journal of Neurology*, vol. 17, no. 6. Wiley-Blackwell, pp. 780–787, 2010. doi: 10.1111/j.1468-1331.2009.02939.x.

[43] G. Kaushik, P. Gaur, R.R. Sharma, R.B. Pachori, EEG signal based seizure detection focused on Hjorth parameters from tunable-Q wavelet sub-bands, *Biomed. Signal Process. Control* 76 (2022) 103645, https://doi.org/10.1016/j.bspc.2022.103645.

[44] S. Das, M. Jabirullah, N. Afreen, A. Prabhakara Rao, and K. V. S. H. Gayatri Sarman, 'Gamma Band: A Bio-Marker to Detect Epileptic Seizures', in *Lecture Notes in Networks and Systems*, Springer Nature Singapore, 2022, pp. 355–364. doi: 10.1007/978-981-19-2764-5_29.

[45] X. Jiang, X. Liu, Y. Liu, Q. Wang, B. Li, L. Zhang, Epileptic seizures detection and the analysis of optimal seizure prediction horizon based on frequency and phase analysis, *Front. Neurosci.* 17 (2023), https://doi.org/10.3389/fnins.2023.1191683.

[46] M. Sameer, A.K. Gupta, C. Chakraborty, B. Gupta, Epileptical Seizure Detection: Performance analysis of gamma band in EEG signal Using Short-Time Fourier Transform, in: In *2019 22nd International Symposium on Wireless Personal Multimedia Communications (WPMC)*, 2019, pp. 1–6, https://doi.org/10.1109/WPMC48795.2019.9096119.

[47] F. Mormann, et al., 'On the predictability of epileptic seizures', *Clinical neurophysiology : official journal of the International Federation of, Clin. Neurophysiol.* 116 (Apr. 2005) 569–587, https://doi.org/10.1016/j.clinph.2004.08.025.

[48] R. Esteller, J. Echauz, T. Tcheng, B. Litt, and B. Pless, 'Line Length: An Efficient Feature for Seizure Onset Detection', in *2001 Conference Proceedings of the 23rd Annual International Conference of the IEEE Engineering in Medicine and Biology Society*, IEEE, Oct. 2001, pp. 1707–1710.

[49] M. Katz J., 'Fractals and the analysis of waveforms', *Computers in Biology and Medicine*, vol. 18, pp. 145–156, 1988.

[50] R. Nagarajan, Quantifying physiological data with Lempel-Ziv complexity-certain issues, *IEEE Trans. Biomed. Eng.* 49 (11) (Nov. 2002) 1371–1373, https://doi.org/10.1109/tbme.2002.804582.

[51] F. Shaffer and P. Ginsberg J, 'An Overview of Heart Rate Variability Metrics and Norms. Front Public Health', *Frontiers in public health*, vol. 5, p. 258, 2017.

[52] M. Malik, Heart rate variability: standards of measurement, physiological interpretation, and clinical use, *Eur. Heart J.* 17 (3) (1996) 354–381, https://doi.org/10.1093/oxfordjournals.eurheartj.a014868.

[53] C.-H. Hsu *et al.*, 'Poincaré plot indexes of heart rate variability detect dynamic autonomic modulation during general anesthesia induction.', *Acta Anaesthesiol Taiwan*, vol. 50, no. 1, pp. 12–18, Mar. 2012, doi: 10.1016/j.aat.2012.03.002.

[54] C.L. Webber Jr, J.P. Zbilut, Recurrence quantification analysis of nonlinear dynamical systems, *Tutorials in Contemporary Nonlinear Methods for the Behavioral Sciences* 94 (2005) (2005) 26–94.
[55] L. Billeci, D. Marino, L. Insana, G. Vatti, M. Varanini, Patient-specific seizure prediction based on heart rate variability and recurrence quantification analysis, *PLoS One* (2018) 1–21.
[56] R.M. Bryce, K.B. Sprague, Revisiting detrended fluctuation analysis, *Sci. Rep.* 2 (1) (Mar. 2012) 315, https://doi.org/10.1038/srep00315.
[57] E. Ihlen, Introduction to Multifractal Detrended Fluctuation Analysis in Matlab, *Front. Physiol.* 3 (2012), https://doi.org/10.3389/fphys.2012.00141.
[58] P.C. Ivanov, et al., Multifractality in human heartbeat dynamics, *Nature* 399 (6735) (Jun. 1999) 461–465, https://doi.org/10.1038/20924.
[59] R. Sassi, M. G. Signorini, and S. Cerutti, 'Multifractality and heart rate variability', *Chaos (Woodbury, N.Y.)*, vol. 19, p. 028507, Jul. 2009, doi: 10.1063/1.3152223.
[60] E. Lake D., S. Richman J., P. Griffin M., and R. Moorman J., 'Sample entropy analysis of neonatal heart rate variability', *American Journal of Physiology-Regulatory, Integrative and Comparative Physiology*, vol. 283, 2002.
[61] J. Yang, G.I. Choudhary, S. Rahardja, P. Franti, Classification of interbeat interval time-series using attention entropy, *IEEE Trans. Affect. Comput.* (2020), https://doi.org/10.1109/TAFFC.2020.3005138.
[62] M. Hubert, M. Debruyne, and P. Rousseeuw, 'Minimum covariance determinant and extensions', *WIREs Computational Statistics*, p. e1421, 2017.
[63] F.T. Liu, K.M. Ting, Z.-H. Zhou, 'Isolation Forest', in, *Eighth IEEE International Conference on Data Mining* 2008 (2008) 413–422, https://doi.org/10.1109/ICDM.2008.17.
[64] L. Manevitz, M. Yousef, One-Class SVMs for Document Classification, *J. Mach. Learn. Res.* 2 (Jan. 2001) 139–154, https://doi.org/10.1162/15324430260185574.
[65] M. Breunig, H.-P. Kriegel, R. Ng, and J. Sander, 'LOF: Identifying Density-Based Local Outliers.', in *ACM Sigmod Record*, Jun. 2000, pp. 93–104. doi: 10.1145/342009.335388.
[66] T. Baltrusaitis, C. Ahuja, and L.-P. Morency, 'Multimodal Machine Learning: A Survey and Taxonomy', *CoRR*, vol. abs/1705.09406, 2017, [Online]. Available: http://arxiv.org/abs/1705.09406.
[67] W.J. Youden, Index for rating diagnostic tests, *Cancer* 3 (1) (1950) 32–35, https://doi.org/10.1002/1097-0142(1950)3:1<32::aid-cncr2820030106>3.0.co;2-3.
[68] B.R. Greene, G.B. Boylan, R.B. Reilly, P. de Chazal, S. Connolly, Combination of EEG and ECG for improved automatic neonatal seizure detection, *Clin. Neurophysiol.* 118 (2007) 1348–1359.
[70] E.P. Salant, A.J. Gabor, D. Leifer, Prediction of epileptic seizures, *Epilepsia* 39 (1998) 1309–1318, https://doi.org/10.1111/j.1528-1157.1998.tb01473.x.
[71] P. Rajdev, M.P. Ward, J. Rickus, R. Worth, P.P. Irazoqui, Real-time seizure prediction from local field potentials using an adaptive Wiener algorithm, *Comput. Biol. Med.* 40 (2010) 97–108, https://doi.org/10.1016/j.compbiomed.2009.11.005.
[72] A. Shafique, M. Sayeed, K. Tsakalis, Nonlinear dynamical systems with chaos and big data: a case study of epileptic seizure prediction and control, in: S. Shah, A. Khan, G. Srivastava (Eds.), *Guide to Big Data Applications*, Springer International Publishing, Cham, Switzerland, 2018, pp. 329–368, https://doi.org/10.1007/978-3-319-53817-4_12.
[73] N.D. Truong, et al., Convolutional neural networks for seizure prediction using intracranial and scalp electroencephalogram, *Neural Netw.* 105 (2018) 104–111, https://doi.org/10.1016/j.neunet.2018.04.018.
[74] S. Kusmakar, C.K. Karmakar, B. Yan, T.J. O'Brien, R. Muthuganapathy, M. Palaniswami, Automated Detection of Convulsive Seizures Using a Wearable Accelerometer Device, *IEEE Trans. Biomed. Eng.* 66 (2) (2019) 421–432, https://doi.org/10.1109/TBME.2018.2845865.
[75] E.B. Motahar, F. Ishtiaque, M.S.I. Wadud, Accelerometer-based Convulsive Seizure Detection using CNN, in: In *2021 IEEE International Conference on Biomedical Engineering, Computer and Information Technology for Health (BECITHCON)*, 2021, pp. 46–51, https://doi.org/10.1109/BECITHCON54710.2021.9893602.
[76] S. Beniczky, I. Conradsen, P. Wolf, Detection of convulsive seizures using surface electromyography, *Epilepsia* 59 (Suppl 1) (2018) 23–29, https://doi.org/10.1111/epi.14048.
[77] M.C. Ortega, E. Bruno, M.P. Richardson, Electrodermal activity response during seizures: A systematic review and meta-analysis, *Epilepsy Behav.* 134 (2022) 108864, https://doi.org/10.1016/j.yebeh.2022.108864.
[78] J. Jeppesen, S. Beniczky, P. Johansen, P. Sidenius, A. Fuglsang-Frederiksen, Exploring the capability of wireless near infrared spectroscopy as a portable seizure detection device for epilepsy patients, *Seizure* 26 (2015) 43–48, https://doi.org/10.1016/j.seizure.2015.01.015.
[79] K. Vandecasteele, et al., Automated Epileptic Seizure Detection Based on Wearable ECG and PPG in a Hospital Environment, *Sensors* 10 (2017) 2338.
[80] T. Karácsony, A.M. Loesch-Biffar, C. Vollmar, J. Rémi, S. Noachtar, J.P.S. Cunha, Novel 3D video action recognition deep learning approach for near real time epileptic seizure classification, *Sci. Rep.* 12 (1) (2022) 19571, https://doi.org/10.1038/s41598-022-23133-9.

Further reading

[69] U.R. Acharya, Y. Hagiwara, H. Adeli, Automated seizure prediction, *Epilepsy Behav.* 88 (2018) 251–261, https://doi.org/10.1016/j.yebeh.2018.09.030.